

IMPROVED FINITE ELEMENT FORMS FOR THE SHALLOW-WATER WAVE EQUATIONS

R. T. WILLIAMS

Department of Meteorology, Naval Postgraduate School, Monterey, California 93940, U.S.A.

O. C. ZIENKIEWICZ†

Department of Mechanical Engineering, Naval Postgraduate School, Monterey, California 93940, U.S.A.

SUMMARY

This paper presents new finite element formulations of the shallow-water wave equations which use different basis functions for the velocity and height fields. These arrangements are analysed with the Fourier transform technique which was developed by Schoenstadt,¹ and they are also compared with other finite difference and finite element schemes. The new schemes are integrated in time for two initial states and compared with analytic solutions and numerical solutions from other schemes. The behaviour of the new forms is excellent and they are also convenient to apply in two dimensions with triangular elements.

KEY WORDS Waves Mixed Finite Element Shallow Water

1. INTRODUCTION

Winninghoff,² Arakawa and Lamb³ and Schoenstadt¹ have demonstrated the superiority of spatial staggering of dependent variables in finite difference formulations of the shallow water equations in a rotating co-ordinate system. These staggered formulations give much better solutions when there are small scale initial conditions or small scale forcing. Also the phase speeds of the inertial-gravity waves are more accurate when an appropriate staggered grid is used. Staggered finite difference schemes are now widely used in meteorology and oceanography. Schoenstadt¹ found similar results with finite element formulations with piecewise linear basis functions. In particular the arrangement with velocity nodal points midway between height nodal points in one dimension is far superior to the usual arrangement with coincident nodal points. However this arrangement with staggered basis functions is not convenient to use especially in two dimensions with irregular geometry.

In this paper an alternative formulation will be presented which uses different basis functions for height and velocity. One of the basis functions is piecewise constant while the other is piecewise linear. They are arranged so that the linear portion of the latter covers the same domain as one of the former functions. This greatly simplifies the application of the method in two-dimensional irregular domains. It will be shown that the linearized FEM equations give excellent solutions when applied to the geostrophic adjustment problem. The time continuous equations will be analysed with the Fourier transform method developed by

† Permanent position: Head, Department of Civil Engineering, University College of Swansea, Swansea, SA2 8PP, United Kingdom.

Schoenstadt,^{1,4} and compared with other finite difference and finite element schemes. The various schemes will be integrated numerically for a particular set of initial conditions, and compared to the exact solution. Advective effects with a mean flow will be investigated with the two finite element arrangements.

2. FORMULATION

The linearized shallow-water equations with constant mean flow U can be written:

$$\frac{\partial u}{\partial t} + U \frac{\partial u}{\partial x} - fv + g \frac{\partial h}{\partial x} = 0, \quad (1)$$

$$\frac{\partial v}{\partial t} + U \frac{\partial v}{\partial x} + fu = 0, \quad (2)$$

$$\frac{\partial h}{\partial t} + U \frac{\partial h}{\partial x} + H \frac{\partial u}{\partial x} = 0, \quad (3)$$

where u and v are the perturbation velocities in the x - and y -directions, and H and h the mean and perturbed heights of the free surface. Also f is the Coriolis parameter and g represents gravity. All quantities are assumed independent of y , although H varies according to $U = -f^{-1}g\partial H/\partial y$. In addition the term $v\partial H/\partial y$ is neglected in (3); this term is only important for very large scale flow.

In the Galerkin formulation the dependent variables are approximated with the basis functions $\varphi_i(x)$ and $\theta_i(x)$ as follows:

$$u(x, t) = u_i(t)\varphi_i(x), \quad v(x, t) = v_j(t)\varphi_j(x), \quad h(x, t) = h_j(t)\theta_j(x), \quad (4)$$

where the repeated index indicates a summation from 1 to N . With these representations, equations (1) and (2) are required to be orthogonal to $\varphi_i(x)$, and (3) is required to be orthogonal to $\theta_i(x)$, which gives:

$$\frac{\partial u_i}{\partial t} \int_0^L \varphi_i \varphi_j dx = -U u_j \int_0^L \varphi_i \frac{\partial \varphi_j}{\partial x} dx - g h_j \int_0^L \varphi_i \frac{\partial \theta_j}{\partial x} dx + f v_j \int_0^L \varphi_i \varphi_j dx, \quad (5)$$

$$\frac{\partial v_j}{\partial t} \int_0^L \varphi_i \varphi_j dx = -U v_j \int_0^L \varphi_i \frac{\partial \varphi_j}{\partial x} dx - f u_j \int_0^L \varphi_i \varphi_j dx, \quad (6)$$

$$\frac{\partial h_j}{\partial t} \int_0^L \theta_i \theta_j dx = -U h_j \int_0^L \theta_i \frac{\partial \theta_j}{\partial x} dx - H u_j \int_0^L \theta_i \frac{\partial \varphi_j}{\partial x} dx. \quad (7)$$

Here i ranges from 1 to N and all fields are periodic in x over distance L .

The two basis functions for arrangement I are given in Figure 1, where $\varphi_i(x)$ is piecewise linear and $\theta_i(x)$ is piecewise constant. Note that $\varphi_i(x)$ is centred at $x = i\Delta x$ while $\theta_i(x)$ is centred at $x = (i + 1/2)\Delta x$. It will be shown that this arrangement has the same advantages as a formulation with piecewise linear basis functions which are staggered. With this arrangement the constant portion of θ_i covers the same space as one of the linear portions of φ_i . This will be a great advantage in two dimensions when the domain is broken into say triangular elements. When the basis functions shown in Figure 1 are introduced into (5)–(7), the

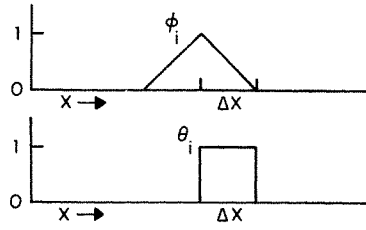


Figure 1. Basis functions for arrangement I

prediction equations become:

Arrangement I

$$M_{ij} \frac{\partial u_j}{\partial t} = -U \frac{u_{i+1} - u_{i-1}}{2\Delta x} - g \left(\frac{h_i - h_{i-1}}{\Delta x} \right) + fM_{ij}v_j, \quad (8)$$

$$M_{ij} \frac{\partial v_j}{\partial t} = -U \frac{v_{i+1} - v_{i-1}}{2\Delta x} - fM_{ij}u_j, \quad (9)$$

$$\frac{\partial h_i}{\partial t} = -U \frac{h_{i+1} - h_{i-1}}{2\Delta x} - H \left(\frac{u_{i+1} - u_i}{\Delta x} \right), \quad (10)$$

where $M_{ij}u_i = (1/6)u_{i+1} + (2/3)u_i + (1/6)u_{i-1}$. The integral in the advection term, $\int \theta_i \partial \theta_j / \partial x dx$, is computed with the modified basis function θ_i^* which is shown in Figure 2. After integration, (see Figure 2), ϵ is allowed to go to zero.

The basis functions for arrangement II, which are obtained by reversing the functions in arrangement I, are shown in Figure 3. When these basis functions are introduced into (4)–(7), the prediction equations become:

Arrangement II

$$\frac{\partial u_i}{\partial t} = -U \frac{u_{i+1} - u_{i-1}}{2\Delta x} - g \left(\frac{h_i - h_{i-1}}{\Delta x} \right) + fv_i, \quad (11)$$

$$\frac{\partial v_i}{\partial t} = -U \frac{v_{i+1} - v_{i-1}}{2\Delta x} - fu_i, \quad (12)$$

$$M_{ij} \frac{\partial h_j}{\partial t} = -U \frac{h_{i+1} - h_{i-1}}{2\Delta x} - H \frac{u_{i+1} - u_i}{\Delta x}, \quad (13)$$

where the procedure involving the special basis function shown in Figure 2 is also required to obtain (11) and (12).

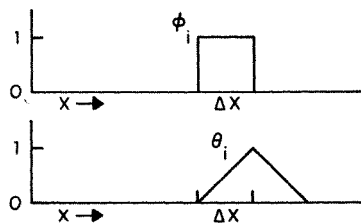


Figure 2. Modified basis functions used for advection terms

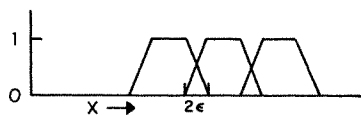


Figure 3. Basis functions for arrangement II (2ϵ —overlap region)

Arrangements I and II give identical equations if mass lumping is carried out, that is when the mass matrix M_{ij} is replaced by the identity matrix I_{ij} . These mass lumped equations are exactly the same as the equations obtained with finite difference scheme B, which has height points equidistant between velocity points. Winninghoff,² Arakawa and Lamb,³ and Schoenstadt¹ have shown that scheme B handles small scale noise very well. Also Schoenstadt¹ has demonstrated that this scheme is superior to a finite element formulation with unstaggered, piecewise linear basis functions.

3. FOURIER TRANSFORM ANALYSIS

In this section we will apply the Fourier transform analysis technique that was developed by Schoenstadt^{1,4} for the geostrophic adjustment problem. This will allow comparisons with other finite difference and finite element formulations. The geostrophic adjustment process is very important in meteorology and oceanography where most of the larger scale motion fields are in approximate geostrophic balance. The wind is in geostrophic balance when the pressure gradient force and the Coriolis force balance. In system (1)–(3) the geostrophic components are

$$u_g = -f^{-1}g \frac{\partial h}{\partial y} = 0, \quad v_g = f^{-1}g \frac{\partial h}{\partial x}.$$

When the initial conditions are not in geostrophic balance, inertial gravity waves will be excited which propagate away from the region of initial imbalance. If the region of initial imbalance is confined, a steady state will be reached which is in geostrophic balance. It is very important that a numerical weather prediction model properly stimulate this process. An example will be presented in Section 4 with numerical solutions from various schemes.

In order to analyse this process following Schoenstadt⁴ the equation set (1)–(3) is Fourier transformed in x which gives:

$$\frac{d\tilde{u}}{dt} = f\tilde{v} - ikg\tilde{h}, \quad (14)$$

$$\frac{d\tilde{v}}{dt} = -f\tilde{u}, \quad (15)$$

$$\frac{d\tilde{h}}{dt} = -ikH\tilde{u}, \quad (16)$$

where

$$\tilde{u}(k, t) = \int_{-\infty}^{\infty} u(x, t) e^{-ikx} dx, \quad (17)$$

and similarly for \tilde{v} and \tilde{h} . This portion of the analysis is simplified by setting $U=0$.

Schoenstadt⁴ solved these equations subject to initial conditions by the eigenvalue-eigenvector approach which gives:

$$\bar{u}(k, t) = \bar{u}_0 \cos \nu t + f \frac{\bar{v}_0}{\nu} \sin \nu t - \frac{ikgh_0}{\nu} \sin \nu t, \quad (18)$$

$$\bar{v}(k, t) = -\frac{f}{\nu} \sin \nu t + \left[\frac{k^2 gH}{\nu^2} + \frac{f^2}{\nu^2} \cos \nu t \right] \bar{v}_0 + \frac{igkf}{\nu^2} [1 - \cos \nu t] \bar{h}_0, \quad (19)$$

$$\bar{h}(k, t) = -\frac{ikH}{\nu} \bar{u}_0 \sin \nu t - \frac{ikfH}{\nu^2} [1 - \cos \nu t] \bar{v}_0 + \left[\frac{f^2}{\nu^2} + \frac{k^2 gH}{\nu^2} \cos \nu t \right] \bar{h}_0, \quad (20)$$

where:

$$\nu^2 = f^2 + k^2 gH. \quad (21)$$

The finite element equation sets (8)–(10) and (11)–(13) can be transformed following Schoenstadt¹ and written in the following general form:

$$\alpha \frac{d\bar{u}}{dt} = \alpha f \bar{v} - i\mu g \bar{h}, \quad (22)$$

$$\alpha \frac{d\bar{v}}{dt} = -\alpha f \bar{u}, \quad (23)$$

$$\gamma \frac{d\bar{h}}{dt} = -i\mu H \bar{u}, \quad (24)$$

where the coefficients α , γ and μ for arrangements I and II are given in Table I. This analysis is easily carried out by noting for example that the transform of h_{i+1} is equal to $\bar{h} e^{ik\Delta x}$ etc. When these equations are solved subject to initial conditions the following set of solutions is obtained:

$$\bar{u} = \bar{u}_0 \cos \nu t - \frac{i\mu g h_0}{\alpha \nu} \sin \nu t + \frac{f \bar{v}_0}{\nu} \sin \nu t \quad (25)$$

$$\bar{v} = \frac{ifg\mu}{\nu^2} (1 - \cos \nu t) \bar{h}_0 - \frac{f}{\nu} \sin \nu t \bar{u}_0 + \left[\frac{\mu^2 gH}{\alpha \gamma \nu^2} + \frac{f^2}{\nu^2} \cos \nu t \right] \bar{v}_0, \quad (26)$$

$$\bar{h} = \left[\frac{\mu^2 gH}{\alpha \gamma \nu^2} \cos \nu t + \frac{f^2}{\nu^2} \right] \bar{h}_0 + \frac{i\mu f H \bar{v}_0}{\gamma \nu^2} (\cos \nu t - 1) - \frac{\bar{u}_0 i\mu H \sin \nu t}{\gamma \nu}, \quad (27)$$

where

$$\nu^2 = f^2 + \frac{\mu^2 gH}{\alpha \gamma}. \quad (28)$$

The comparison of these solutions with the exact solutions (18)–(20) shows that they have the same form, but various coefficients are modified by spatial truncation error. The exact

Table I

Arrangement	α	γ	μ
Differential	1	1	k
I	$(2 + \cos k\Delta x)/3$	1	$\sin(k\Delta x/2)/(\Delta x/2)$
II	1	$(2 + \cos k\Delta x)/3$	$\sin(k\Delta x/2)/(\Delta x/2)$

Table II

Differential (18)–(20)	$1/\nu$	k/ν	k/ν^2
Finite element (25)–(27)	$1/\nu$	$\mu/\alpha\nu, \mu/\gamma\nu, \mu/\sqrt{(\alpha\gamma\nu)}$	$\mu/\alpha\nu^2, \mu/\gamma\nu^2$

coefficients dependent on $1/\nu$, k/ν and k/ν^2 and the corresponding expressions for the finite element schemes are given in Table II. The exact frequency is given by (21), while the finite element form is given by (28). When the relations in Table I are used in the latter equation, it can be seen that ν is the same for arrangements I and II. The other terms such as $\mu/\alpha\nu$ and $\mu/\gamma\nu$ show no obvious advantage for either arrangement because the formulas for α and γ are merely interchanged between the two arrangements. In Section 5 these arrangements will be compared with other schemes by integrating the equations in time from a particular initial state, and some differences will be noted in the final velocity field.

It is useful to compare the phase speed and group velocity obtained from these basis function arrangements with other finite element and finite differences formulations. Figure 4(a) contains the phase velocity $c = \nu/k$ as a function of $k\Delta x/\pi$. The figure includes curves for the following: 1 analytic solution; 2 finite difference scheme A; 3 FEM scheme A; 4 finite difference scheme B; 5 FEM scheme B; 6 arrangements I and II. Curves 1–5 in Figures 4 and 5 are taken from Schoenstadt.¹ Finite difference scheme A carries u , v and h at all

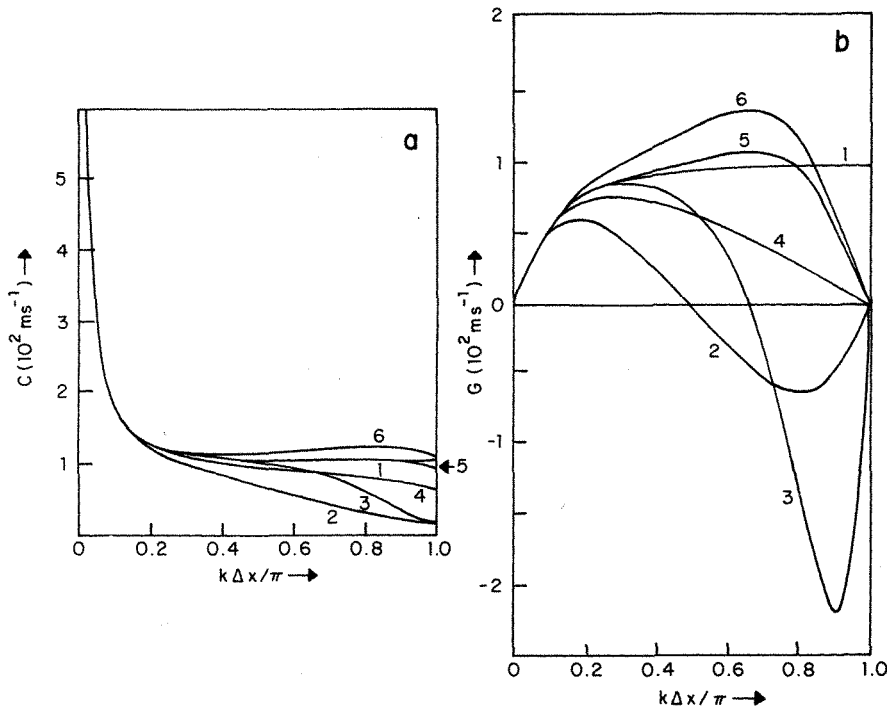


Figure 4. The phase velocity $c = \nu/k$, and the group velocity $G = d\nu/dk$ as functions of $k\Delta x/\pi$ for the various schemes. The curve numbering is given in the text. These results use the following values: $gH = 10^4 \text{ m}^2 \text{ s}^{-2}$, $f = 10^{-4} \text{ s}^{-1}$, $\Delta x = 500 \text{ km}$

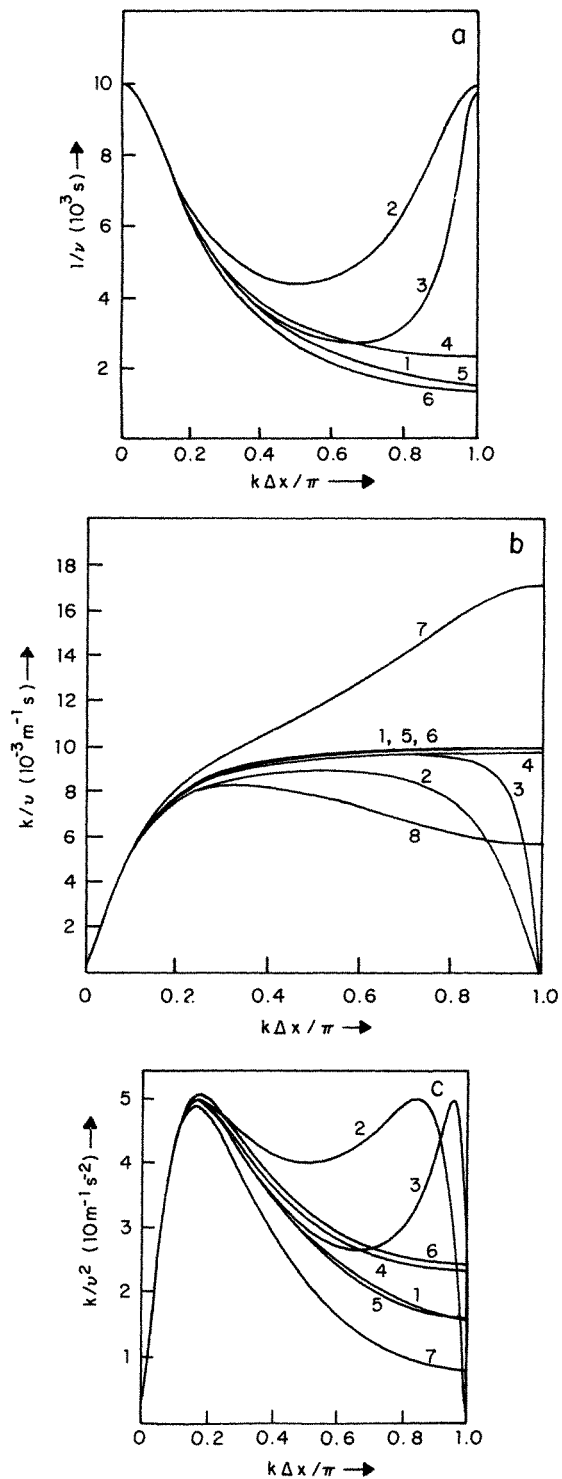


Figure 5. The coefficients $1/\nu$, k/ν and k/ν^2 as functions of $k\Delta x/\pi$ for the same conditions used in Figure 4

points and FEM scheme A uses piecewise linear basis functions for u , v and h . Finite difference scheme B places u , v grid points between h points and FEM scheme B employs piecewise linear basis functions with the u , v nodal points equidistant between the h nodal points. The analytic solution (curve 1) approaches f/k for small k and $(gH)^{1/2}$ for large k . Scheme A (curve 2) gives the poorest phase speed and FEM scheme A (curve 3) is also very poor for the highest wave numbers. The FEM scheme B (curve 5) is very close to the analytic solution. Arrangements I and II (curve 6) also give excellent phase velocities. If arrangements I and II are mass-lumped they reduce to scheme B (curve 4) which is better than the unstaggered schemes.

The group velocity $G = d\nu/dk$ is given in Figure 4(b) for the same schemes. The analytic solution is zero at $k=0$ and it approaches $(gH)^{1/2}$ for large k . Scheme A (curve 2) and its finite element version (curve 3) are very poor for the short waves (large k) since they propagate energy in the wrong direction. The best group velocity is for FEM scheme B (curve 5), but arrangements I and II (curve 6) are also good.

The coefficients given in Table II which correspond to $1/\nu$, k/ν is given in Figure 4(b) for the same schemes. The analytic solution is zero at $k=0$ and it approaches $(gH)^{1/2}$ for large k . Scheme A (curve 2) and its finite element version (curve 3) are very poor for the short waves (large k) since they propagate energy in the wrong direction. The best group velocity is for FEM scheme B (curve 5), but arrangements I and II (curve 6) are also good.

The coefficients given in Table II which correspond to $1/\nu$, k/ν and k/ν^2 are given in Figures 5(a), 5(b) and 5(c). The first figure, which includes the same schemes as Figure 4, is important because $1/\nu^2$ relates the initial height to the final steady state height [see (20)]. Scheme A (curve 2) and FEM scheme A (curve 3) are very poor for the shortest waves. In fact if $\tilde{v}_0 = 0$ the final h for $k = \pi/\Delta x$ is more than 25 times too large for these schemes. This illustrates the production of small scale noise by non-staggered grids. All of the staggered schemes are much better, and the best is FEM scheme B (curve 5). Arrangements I and II also give excellent solutions.

Figure 5(b) shows the representations of k/ν for various schemes, but as is indicated in Table II, arrangements I and II each have three representations. The quantity $\mu/\sqrt{\alpha\gamma\mu}$, which is the same for both arrangements, is curve 6. The terms $\mu/\alpha\nu$ and $\mu/\gamma\nu$ for arrangement I are represented by curves 7 and 8 respectively. These terms for arrangement II are obtained by interchanging the curves since α and γ are interchanged. As with the previous figures schemes A and FEM A are the poorest and FEM scheme B is the best. Curve 6 for $\mu/\sqrt{\alpha\gamma\nu}$ is very good, but curves 7 and 8 for $\mu/\alpha\nu$ and $\mu/\gamma\nu$ are poor. However, as may be seen in (25) and (27) these coefficients do not affect the final steady state and they are related to either u or its initial value. Thus the unusual behaviour of these coefficients should have little effect on the geostrophic adjustment process and no effect on the final steady state.

Figure 5(c) contains the representations of k/ν^2 for the various schemes including the corresponding terms $\mu/\alpha\nu^2$ and $\mu/\gamma\nu^2$ for arrangements I and II (see Table II). The worst curves are for schemes A and FEM A, and the best is for FEM scheme B. Curve 6 gives $\mu/\alpha\nu^2$ and curve 7 $\mu/\gamma\nu^2$ for arrangement I, and the curves are interchanged for arrangement II. These curves lie on both sides of the analytic curve and they represent about the same error as with scheme B (curve 4). These coefficients are important because they appear in expressions for h and v , and because they affect the steady state solutions.

The analyses of this section show that the unstaggered finite difference and finite element schemes are poor for small scales with respect to phase speed, group velocity and final adjusted structure. The best scheme is the staggered finite element formulation with piecewise linear basis functions. However, the mixed basis function arrangements introduced

in this paper also do very well, and they give the same curves in Figure 4 and Figure 5(a) as were obtained by Williams⁵ for a FEM vorticity-divergence formulation.

4. NUMERICAL EXAMPLE OF GEOSTROPHIC ADJUSTMENT

In this section the various schemes, which were examined in Section 3, will be compared by direct numerical integration in x and t . Two aspects of the geostrophic adjustment process must be considered in assessing a particular numerical scheme: (i) forecast time required to reach the adjusted state; (ii) the accuracy of the final adjusted state. The group velocity curves in Figure 4(a) provide an indication of the comparative adjustment times for the various schemes. The final adjusted state, which is more important, could be obtained by Fourier transforming the terms that are independent of t in (25)–(27). However, in this paper the final state will be determined by integrating the finite difference equations in t until the adjusted state is reached. This approach is preferable because time differencing effects are included and a time filter can be used.

The various schemes are integrated by introducing centred time differences, and the time filter developed by Robert⁶ (see also Asselin⁷) is applied to the past time value with the coefficient $\gamma = 0.05$. The FEM schemes use Gauss elimination to invert the mass matrix.

The initial conditions are given by:

$$h(x, 0) = \begin{cases} a & |x| \leq \Delta x/2 \\ 0 & |x| > \Delta x/2, \end{cases} \quad (29)$$

$$u(x, 0) = v(x, 0) = 0.$$

The analytic solution for the final adjusted h field is given by the following expression which was derived by Schoenstadt:⁴

$$h_s(x) = h(x, 0) - \frac{H}{2L_R^2 f} \int_{-\infty}^{\infty} \text{sgn}(x - \xi) e^{-|x - \xi|/L_R} \left[\frac{g}{f} \frac{\partial h}{\partial x}(\xi, 0) - v(\xi, 0) \right] d\xi, \quad (30)$$

where h_s is the final adjusted height and $L_R = (gH)^{1/2} f$ is the Rossby radius of deformation. Also $\text{sgn}(x)$ means the sign of x . The initial geostrophic wind which is required in (30) can be written:

$$\frac{g}{f} \frac{\partial h}{\partial x}(x, 0) = \frac{ag}{f} [\delta(x + \Delta x/2) - \delta(x - \Delta x/2)], \quad (31)$$

where $\delta(x)$ is the delta function.

When (29) and (31) are introduced into (30), the height solution becomes:

$$h_s(x) = a \begin{cases} e^{-x/L_R} \sinh(\Delta x/2L_R) & \Delta x/2 < x \\ 1 - e^{-\Delta x/2L_R} \cosh(x/L_R) & -\Delta x/2 \leq x \leq \Delta x/2 \\ e^{x/L_R} \sinh(\Delta x/2L_R) & x < -\Delta x/2 \end{cases} \quad (32)$$

This analytic solution is given in Figure 6. The solution for the northward component is obtained from the geostrophic condition $v_s = f^{-1} g \partial h_s / \partial x$ as follows:

$$v_s = a \sqrt{(g/H)} \begin{cases} -e^{-x/L_R} \sinh(\Delta x/2L_R) & \Delta x/2 < x \\ -e^{-\Delta x/2L_R} \sinh(x/L_R) & -\Delta x/2 \leq x \leq \Delta x/2 \\ e^{x/L_R} \sinh(\Delta x/2L_R) & x < -\Delta x/2 \end{cases} \quad (33)$$

This analytic solution is included in Figure 7 for $x > 0$.

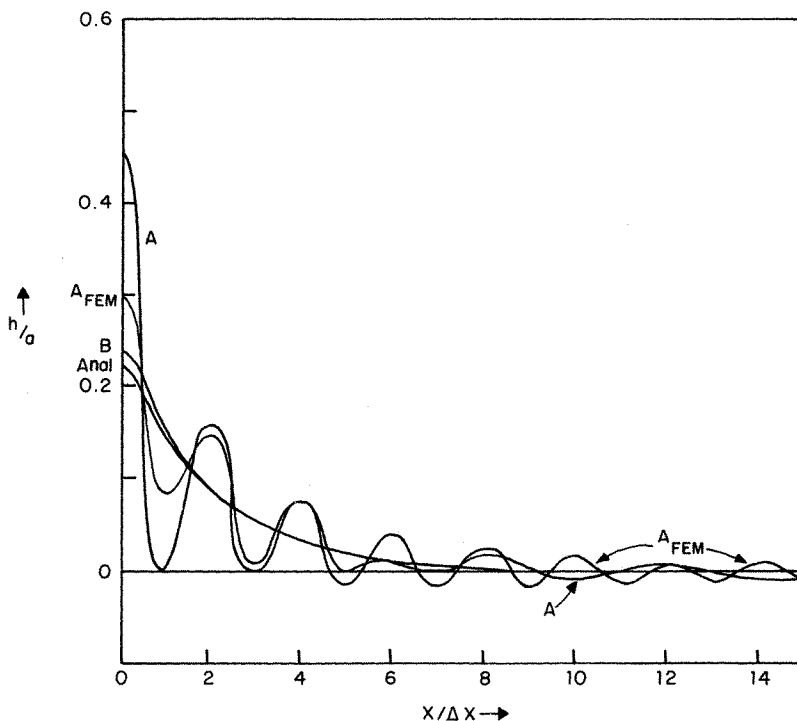


Figure 6. The h solutions for schemes A, B and FEM A functions of $x/\Delta x$ at $t=3$ days. The steady-state analytic solution, which is given by (32) is also included

The numerical integrations with the various schemes are performed on a grid of 200 points with cyclic boundary conditions. The initial disturbance at $x=0$ is placed in the centre of the computational domain so that the cyclic boundary conditions will not affect the solution near $x=0$ until well after the adjusted state is reached. For each scheme the initial disturbance is placed at a single point although formal application of the Galerkin procedure to (4) could affect other points. Figure 6 includes the numerical solution at $t=3$ days for the following schemes: A, B and FEM A. Scheme A shows strong oscillations with every other point returning to 0. FEM A has smaller oscillations near $x=0$, but they become larger than the oscillations for scheme A further out. This is apparently caused by the spuriously large group velocity. Scheme B gives very smooth behaviour and it is close to the analytic solution. Table III compares the solutions for all of the schemes at $x=0$ and $x=\Delta x$. The best schemes are FEM B and arrangements I and II. The behaviour of the various schemes (Figure 6 and Table III) is consistent with the curves for $1/\nu$ shown in Figure 5(a), since \hat{h}_s is proportional to $1/\nu^2$ [see (20)].

Figure 7 includes some of the numerical solutions for v at $t=3$ days as well as the analytic solution given by (33). Only the positive x variation is shown since the solutions are odd functions of x . The analytic solution has extremes at $x=\pm\Delta x/2$ and decays exponentially for large $|x|$. The solutions for schemes A and FEM A show large oscillations as was seen for the h field in Figure 6. Arrangements I and II give much better solutions, as expected, from their h field which is shown in Figure 6. However, arrangement I gives an extremely accurate solution at point $x=\Delta x/2$. This can be explained by first noting that the final state satisfies the geostrophic relation $fv - g \partial h/\partial x = 0$. Arrangement I handles this relation more accurately

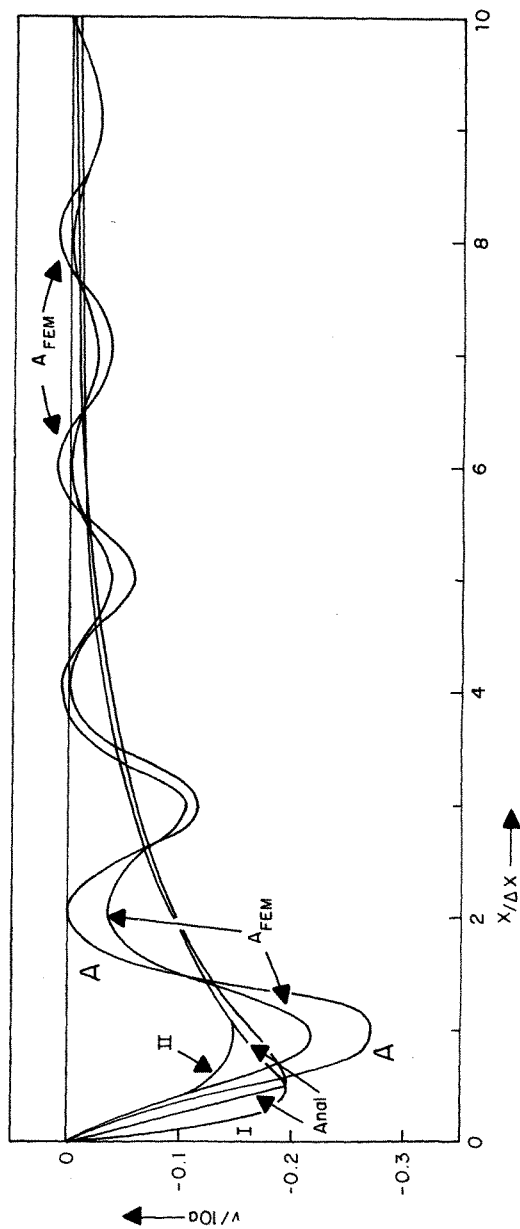


Figure 7. The v solutions for schemes A and FEM A, and for arrangements I and II, as functions of $x/\Delta x$ at $t = 3$ days. The steady-state analytic solution, which is given by (33) is also included

Table III

x	0	Δx
Analytic	0.221	0.153
A	0.459	0.0
FEM A	0.298	0.084
B	0.240	0.148
FEM B	0.227	0.157
Arrangements I, II	0.213	0.154

because it uses the full mass matrix for the Coriolis term fv [see (8) and (11)]. The factor of $1/\alpha$ can be seen in the steady state portions of (26), and in the difference between the curves in Figure 5(c) for arrangements I and II.

5. ADVECTIVE EFFECTS

The advective terms which involve U in equations (1)–(3) are very important in most meteorological and oceanographic problems. These effects were neglected in Sections 3 and 4 which treated the geostrophic adjustment process. Solutions of the form $e^{ik(x-ct)}$ to the set (1)–(3) give the phase velocities

$$c = \begin{cases} U \\ U \pm (gH + f^2/k^2)^{1/2}. \end{cases} \quad (34)$$

The first solution, which corresponds to the steady state solution in Sections 3 and 4, is the most important for many geophysical problems.

Arrangements I and II treat the advective process differently depending on whether or not the full matrix is used in a particular equation. To illustrate this effect consider the simple advection equation,

$$\partial \zeta / \partial t + U \partial \zeta / \partial x = 0. \quad (35)$$

With arrangements I and II this equation is written

$$\frac{1}{6} \frac{\partial \zeta_{i+1}}{\partial t} + \frac{2}{3} \frac{\partial \zeta_i}{\partial t} + \frac{1}{6} \frac{\partial \zeta_{i-1}}{\partial t} + U \frac{(\zeta_{i+1} - \zeta_{i-1})}{2\Delta x} = 0, \quad (36)$$

or

$$\frac{\partial \zeta_i}{\partial t} + U \frac{(\zeta_{i+1} - \zeta_{i-1})}{2\Delta x} = 0, \quad (37)$$

where (36) employs the full mass matrix and (37) is mass lumped. The computational phase speed can be found by substituting $\zeta = A e^{ik(x-c_F t)}$ into each equation and solving for c_F . Equation (36) gives

$$c_F = U \left(\frac{3}{2 + \cos k\Delta x} \right) \frac{\sin(k\Delta x)}{k\Delta x} \quad (38)$$

and (37) gives

$$c_F = U \frac{\sin(k\Delta x)}{k\Delta x}. \quad (39)$$

The analytic solution to (35) is $c = U$ and both (38) and (39) approach U as $\Delta x \rightarrow 0$ for fixed k . Figure 8 contains c_F/U for (38) and (39) as a function of $k\Delta x/\pi$. Clearly the full mass matrix form (36) is much more accurate than the mass-lumped form (37).

In order to compare arrangements I and II for the advective solution $c = U$ it is important to determine whether or not one of the basic equations (1)–(3) is more important than the others for small scale motions. Geostrophic adjustment theory [see for example Section 2.8 in Haltiner and Williams⁸] states that when the initial scale L is less than L_R , the final state is mainly determined by the initial wind field and when L is greater than L_R the final state is mainly determined by the initial height field. The critical scale L_R is called the Rossby radius of deformation and it is given by

$$L_R = (gH)^{1/2}/f. \tag{40}$$

This suggests that when L_R is greater than Δx , the equations of motion (1) and (2) will have more effect on the phase speed than the continuity equation (3). In that case arrangement I should be better because it gives a more accurate treatment of the advective term since it uses the full mass matrix. Conversely when Δx is greater than L_R arrangement II should be superior.

In order to test these ideas, the two schemes will be integrated numerically from a particular initial state for various values of $\Delta x/L_R$. The initial conditions are:

$$\begin{aligned} h(x, 0) &= a \cos^N\left(\frac{\pi x}{W}\right), \\ u(x, 0) &= 0, \\ v(x, 0) &= -\frac{gaN\pi}{fW} \cos^{N-1}\left(\frac{\pi x}{W}\right) \sin\left(\frac{\pi x}{W}\right) = \frac{g}{f} \frac{\partial h(x, 0)}{\partial x}, \end{aligned} \tag{41}$$

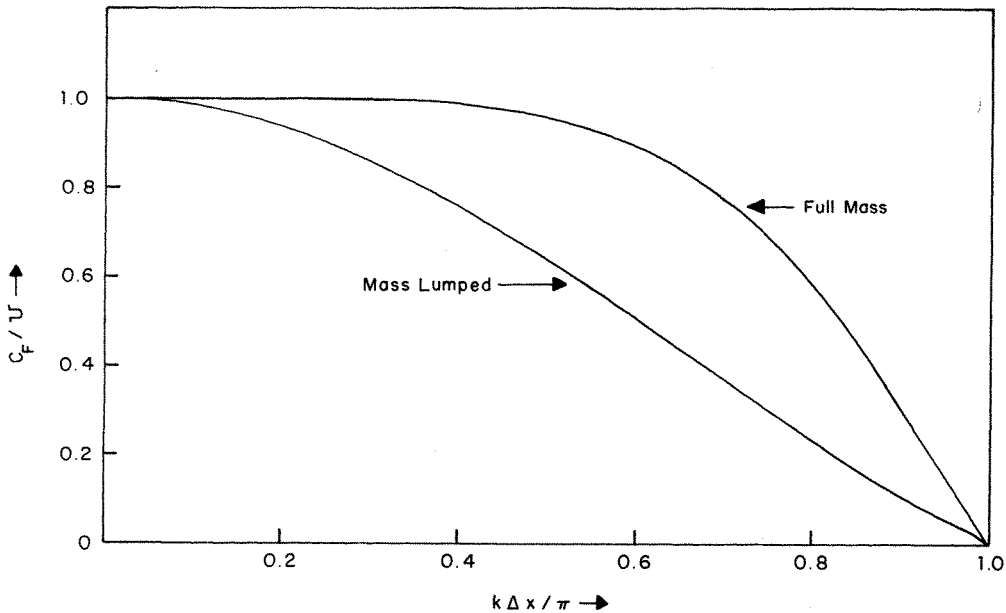
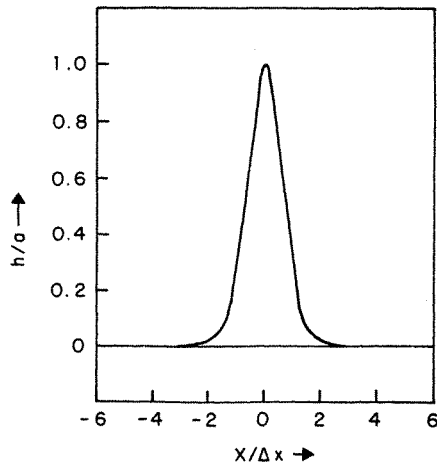


Figure 8. The ratio c_F/U for the full mass matrix (36) and mass lumped (37) forms of the advection equation as functions of $k\Delta x/\pi$

Figure 9. The initial h field as given by (41)

where a is the amplitude and W is the width of the computational domain. The initial v field is geostrophically related to h , which means that the initial field will move with the speed $c = U$ [see (34)]. Figure 9 gives the initial height field for $N = 10\,000$ and $W = 200 \Delta x$. Note that this small scale field has a large height change over one grid length, and it should be very sensitive to the numerical scheme which is used.

Arrangements I and II are integrated for five days using a mean flow of $U = 10 \text{ m s}^{-1}$ with the numerical techniques which were discussed in Section 4. Figure 10 shows the numerical solutions for $\Delta x = 5L_R$ and $\Delta x = L_R/5$ obtained with arrangement I. The exact solution is also included. Generally the numerical solutions move too slowly, have too small amplitude, and contain fictitious short waves. This behaviour occurs because the numerical solutions are

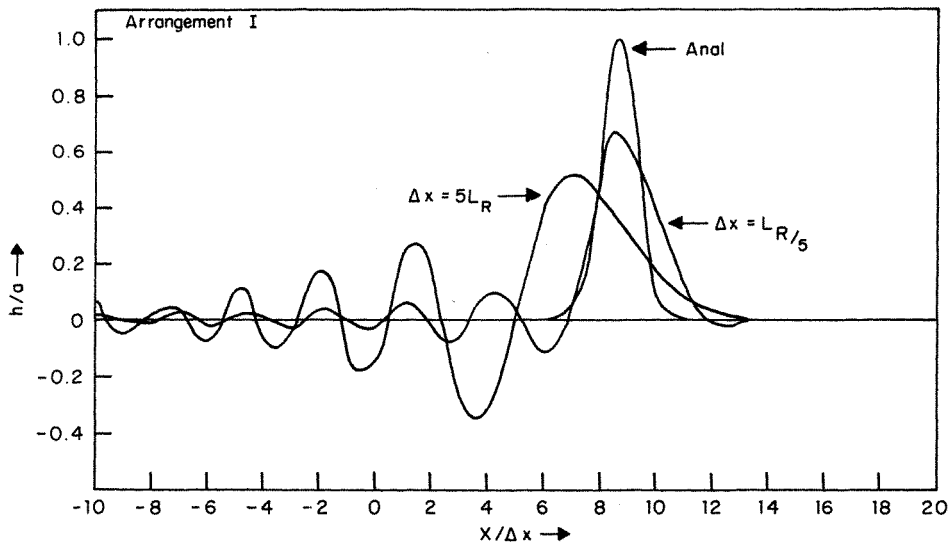


Figure 10. The h solutions for arrangement I for $\Delta x = 5L_R$ and $\Delta x = L_R/5$ at $t = 5$ days with $U = 10 \text{ m s}^{-1}$. The analytic solution is also included. The basic parameters are the same as those used in Figure 4, except that f is varied to give the required changes in L_R

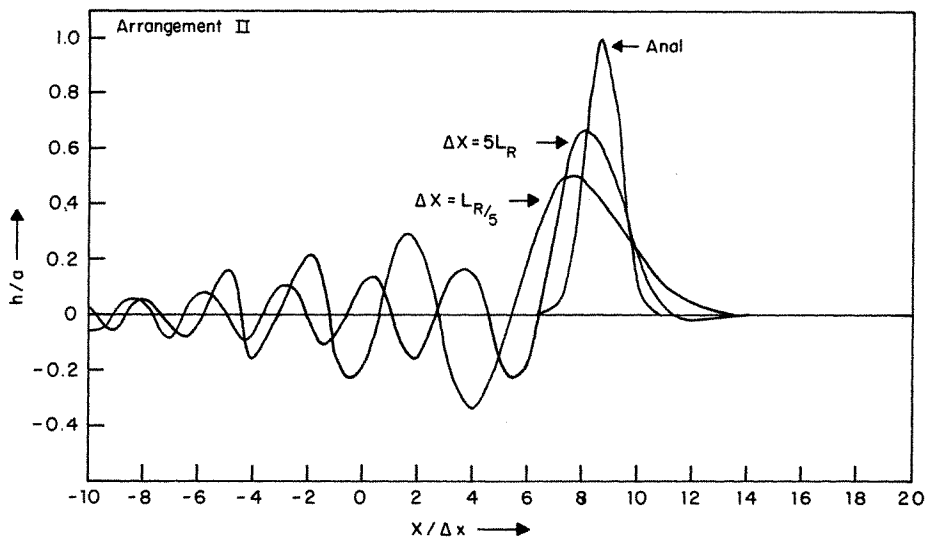


Figure 11. The same as Figure 10 except for arrangement II

falsely dispersive as can be seen in Figure 8. A localized disturbance such as the one shown in Figure 9 is composed of many Fourier components, and if these components have different phase speeds because of numerical truncation, they will begin to move out of phase with each other. This reduces the maximum amplitude and it leads to the appearance of wiggles. The numerical solution also moves too slowly, because each wave is too slow (see Figure 8). In Figure 10 it is seen that the solution with $\Delta x = L_R/5$ is superior to the one with $\Delta x = 5L_R$ as regards to amplitude, phase speed and smallness of wiggles. Figure 11 shows the same fields for arrangement II. In this case the solution for $\Delta x = 5L_R$ is superior to the solution for $\Delta x = L_R/5$. These results are entirely consistent with the discussion presented earlier in this section. Arrangement I should be used when $L_R > \Delta x$ and arrangement II should be used when $L_R < \Delta x$. In most meteorological applications $L_R > \Delta x$, but large scale ocean circulation models do often have $L_R < \Delta x$.

6. CONCLUSIONS

Schoenstadt¹ has developed a technique for analysing finite difference and finite element prediction schemes which are based on the linearized shallow-water equations. The technique treats the geostrophic adjustment problem by applying the spatial Fourier transform to the system of equations. The solutions for arbitrary initial conditions are written in terms of various coefficients which can be evaluated as a function of wave number for each numerical scheme. Schoenstadt¹ analysed a variety of finite difference and finite element schemes and some of his results were reported in this paper. Schoenstadt found that the finite element formulation which uses the same piecewise linear basis functions for all variables (FEM scheme A) is very poor for the shortest wavelengths. However, when the basis functions are staggered in such a way that the velocity nodal points are midway between the height nodal points (FEM scheme B), he found excellent solutions. Similar behaviour was found for finite difference equations as had been previously examined by Winninghoff² and Arakawa and Lamb.³

FEM scheme B handles geostrophic adjustment extremely well, but it would be complicated to apply in two dimensions with the nonuniform, general, elements [such as those discussed by Zienkiewicz⁹]. In this formulation the velocities and the height are represented with different basis functions. In arrangement I piecewise linear basis functions are used for the velocities and piecewise constant for the height. The basis functions are interchanged in arrangement II. These arrangements were examined with the Schoenstadt technique and it was found that both handle the geostrophic adjustment process very well. In particular both arrangements give the same phase speeds and group velocities which are nearly as good as those given by FEM scheme B.

Arrangements I and II and some of the other schemes were integrated with leapfrog time differences as an example. The initial state was at rest with an initial height perturbation at a single point. The equations were integrated until a balanced state was achieved where the pressure gradient force was balanced by the Coriolis force. FEM scheme A provided a very poor solution which falsely oscillated from point to point. The spatially staggered schemes came very close to the analytic steady solution. Arrangement I was excellent and a little better than arrangement II, because it does a better job on the Coriolis terms.

The two arrangements were also compared by integrating the equations with a mean current, and a small scale initial disturbance which was in geostrophic balance. The various integrations showed that arrangement I is more accurate when $L_R > \Delta x$ and arrangement II is better when $L_R < \Delta x$, where L_R is the Rossby radius of deformation.

Although the applications in this paper all include the Coriolis force, it can be expected that arrangements I and II will give excellent results in various nonrotating applications. For example the phase velocities in Figure 4(a) show that arrangements I and II are superior to FEM scheme A for the shorter wavelengths where the Coriolis effects are less important. Arrangements I and II should produce much less small noise than FEM scheme A because the pressure gradient and divergence terms in equations (1) and (3) respectively, are handled more accurately. The two arrangements are now in the process of being tested in nonlinear, two-dimensional versions at the University College of Swansea.

ACKNOWLEDGEMENTS

The authors wish to thank Professor G. J. Haltiner for reading the manuscript and for making useful comments. The research was partially supported by the Naval Air Systems Command through the Naval Environmental Prediction Research Facility.

The numerical computations were performed by the W. R. Church Computer Center. The manuscript was carefully typed by Ms. M. Marks.

REFERENCES

1. A. Schoenstadt, 'A transfer function analysis of numerical schemes used to simulate geostrophic adjustment', *Monthly Weather Review*, **108** (1980).
2. F. Winninghoff, 'On the adjustment toward a geostrophic balance in a simple primitive equation model with application to the problem on initialization and objective analysis', *Doctoral Dissertation*, UCLA 1981, p. 161.
3. A. Arakawa and V. Lamb, 'Computational design of the basic dynamical processes of the UCLA General circulation model', *Methods of Computational Physics*, Academic Press, **17**, 174-266 (1977).
4. A. Schoenstadt, 'The effect of spatial discretization on the steady-state and transient behavior of a dispersive wave equation', *J. Comp. Phys.*, **23**, 364-379 (1977).
5. R. T. Williams, 'On the formulation of finite element prediction models', submitted to *Monthly Weather Review* (1981).

6. A. Robert, 'The integration of a low order spectral form of the primitive meteorological equations', *J. Meteor. Soc. Japan*, **44**, 237-245 (1966).
7. R. Asselin, 'Frequency filter for time interpolations', *Monthly Weather Review*, **100**, 487-490 (1972).
8. G. J. Haltiner and R. T. Williams, *Numerical Prediction and Dynamic Meteorology*, Wiley, New York, 1980, p. 477.
9. O. C. Zienkiewicz, *The Finite Element Method*, McGraw-Hill, London, 1977, p. 787.